RESEARCH ARTICLE

Check for updates

Switchable coordination bonds in 3D cyano-bridged perovskite ferroelastics: achieving the largest leap of symmetry breaking and enhanced dielectric switching performance†

Sheng-Qian Hu, Meng-Zhen Li, Zhao-Hong Chen, Jun-Si Zhou, Luan-Ying Ji, Yong Ai [ID] and Xiao-Gang Chen [ID] *

Three-dimensional (3D) cyano-bridged perovskites, with a larger framework than their metal–halide counterparts, have shown great promise in the design of molecular ferroelastic, ferroelectric, and even multiferroic materials. However, the relatively weak interaction between the organic cations and the rigid cyano-bridged framework usually makes them exhibit a low phase transition temperature (T_c) and inadequate performance. In this study, we used the parent compounds $[C_3H_6NH_2]_2[MFe(CN)_6]$ ($C_3H_6NH_2$ = azetidinium, M = K, Rb or Cs) as starting points to design a variety of 3D cyano-bridged perovskite ferroelastic materials $[C_3H_5FNH_2]_2[MFe(CN)_6]$ ($C_3H_5FNH_2$ = 3-fluoroazetidinium) through the H/F substitution strategy. Notably, in comparison with $[C_3H_6NH_2]_2[MFe(CN)_6]$, the strongest electronegative fluorine atom of $[C_3H_5FNH_2]^+$ cations forms a C–F–M coordination bond with alkali metal ions, which greatly enhances the interaction between the cation and the framework, thus increasing T_c. The transition from order to disorder in $[C_3H_5FNH_2]^+$ cations, coupled with the generation/breakage of switchable C–F–M coordination bonds, synergistically results in the largest leap of symmetry breaking with an Aizu notation of $m\bar{3}mF\bar{1}$ and is responsible for significantly enhancing the dielectric switching performance. This study offers an effective approach for discovering novel molecular ferroelastics with excellent switchable physical properties.

Introduction

Ferroelastic materials are crucial for various potential applications including mechanical switches, shape memory devices, energy conversion systems, information processing technologies, solar cells, and multifunctional superelasticity.[1–8] Organic–inorganic hybrid perovskites (OIHPs), in comparison with their inorganic counterparts, have garnered increasing interest in recent years due to their environmentally friendly nature, ease of processing, mechanical flexibility, affordability, and biocompatibility.[9–26] Their unique structures, where the inorganic component guarantees stability and fascinating electro-optical properties while the organic part provides structural flexibility and variability, offer great potential for constructing and optimizing multifunctional ferroelastic materials.[27–34] Among these, three-dimen-

sional (3D) cyano-bridged perovskites have attracted considerable attention, primarily because many cyanide compounds exhibit an intriguing dielectric property switchability triggered by structural phase transitions.[35–38] In 3D cyano-bridged perovskites, various metal ions can be linked by the cyanide ions to form the striking double perovskite structure, $A_2[B'B''(CN)_6]$ (A = monovalent cation, B'(I) = monovalent metals, such as K^+, Rb^+, and Cs^+, and B''(III) = trivalent metals, such as Fe^{3+} and Co^{3+}). Incorporating cationic A guests into the host cages formed by B'–NC–B'' results in the assembly of a 3D hole structure, making it a highly promising class of switchable molecular dielectrics.[39–42] The mechanisms of dielectric switching in these cyano-bridged OIHP ferroelastics typically arise from the conventional order–disorder transition of the A-site guests.[43–45] In this transition, the ordered state corresponds to a low dielectric constant (referred to as 'switching-off'), whereas the disordered state corresponds to an activated high dielectric constant (referred to as 'switching-on'). However, the larger B'–NC–B'' framework results in a weaker confinement effect for the A-site cations within the cage, leading to a lower T_c and unspectacular symmetry breaking, which makes it difficult to achieve large dielectric switching

Ordered Matter Science Research Center, Nanchang University, 330031, P. R. China. E-mail: chenxg@ncu.edu.cn

This journal is © the Partner Organisations 2024

Inorg. Chem. Front., 2024, **11**, 4647–4653 | **4647**

responses and hinders its application in practical electronic devices.

To address this challenge, Xu *et al.*[46] pioneered the introduction of switchable coordination bonds into this 3D cyano-bridged perovskite system. The generation/breakage of the N–O–K coordination bonds between $[(CH_3)_3NOH]^+$ cations and the $[KFe(CN)_6]^{2-}$ framework led to a significant symmetry breaking with transitioning from the high-temperature cubic non-polar $Fm\bar{3}m$ space group (*No.* 225) to the low-temperature monoclinic polar Cc space group (*No.* 9) in $[(CH_3)_3NOH]_2[KFe(CN)_6]$, thereby yielding a 3D perovskite ferroelectric with both high T_c up to 402 K and excellent multipolar axis properties. Similar properties were also reported by Rok *et al.* in their Co-based analogs.[47] Thus, mastering the structural phase transition mechanism and manipulating the crystal symmetry are essential for obtaining high-performance ferroic materials.[48] However, to date, research on switchable coordination bond ferroelastic materials remains scarce.

Hydrogen/fluorine (H/F) substitution, involving the replacement of an H atom with an F atom in organic cations, minimally disrupts the crystal structure while significantly increasing T_c and has been widely used to construct ferroelectric and ferroelastic materials.[49–52] For instance, employing a fluorine substitution strategy, ferroelectrics like (4-fluoro-1-azabicyclo[2.2.1]heptane)CdCl$_3$, (*R*) and (*S*)-3-(fluoropyrrolidinium)MnCl$_3$, and (*R*) and (*S*)-(*N*,*N*-dimethyl-3-fluoropyrrolidinium) iodide exhibit enhanced T_c, demonstrating the comparable or even superior performance of H/F substitution compared to the isotope effect.[53–55] In contrast to the aforementioned cases, we recently discovered that the strong electronegative F atom in the organic cation can form a coordination bond with K^+ ions from the $[KFe(CN)_6]^{2-}$ framework, which can reduce the symmetry of the parent compound from the tetragonal $I4/m$ space group (*No.* 87) to the monoclinic $C2/c$ space group (*No.* 9).[48] This inspired the development of high-performance switchable coordination bond ferroelastic materials.

In this study, we successfully devised and synthesized a series of 3D cyano-bridged perovskite ferroelastics, denoted as $[C_3H_5FNH_2]_2[MFe(CN)_6]$, which we named FAZT-K, FAZT-Rb, and FAZT-Cs when M = K, Rb, and Cs, respectively. This was achieved *via* H/F substitution starting from the parent compounds $[C_3H_6NH_2]_2[MFe(CN)_6]$, referred to as AZT-K, AZT-Rb, and AZT-Cs, respectively (Scheme 1). Notably, the establishment of switchable C–F–M coordination bonds between the $[C_3H_5FNH_2]^+$ cations and the $[MFe(CN)_6]^{2-}$ framework not only played a significant role in enhancing T_c, but also led to the largest leap of symmetry breaking with the Aizu notation of $m\bar{3}mF\bar{1}$ among the 3D cyano-bridged perovskites (Fig. S1 and Table S1, ESI†). Among them, FAZT-Rb exhibits favorable dielectric switching performance with ΔT_c as high as 132 K, and a ratio of dielectric switching of up to 5. To our knowledge, this method of achieving the effect of killing three birds with one stone, that is, simultaneously increasing T_c, improving the switchable dielectric response, and intensifying the symmetry breaking, is unprecedented in the design of molecular ferroelastic materials.

Results and discussion

Differential scanning calorimetry (DSC)

All compounds were obtained by evaporating the aqueous solution at a slow rate, resulting in reddish-brown block-like crystals (Fig. S2, ESI†), demonstrating excellent thermal stability up to 500 K, except for FAZT-Cs as indicated by TGA analyses (Fig. S3, ESI†). Powder X-ray diffraction measurement at room temperature confirmed their good phase purity (Fig. S4, ESI†). Differential scanning calorimetry (DSC) measurements conducted at a rate of 20 K min^{-1} revealed the phase transitions of FAZT-K, FAZT-Rb, and FAZT-Cs at around 295 K, 350 K, 379 K (T_{c1} of FAZT-Cs), and 394 K (T_{c2} of FAZT-Cs), respectively (Fig. 1a). The T_c of $[C_3H_5FNH_2]_2[MFe(CN)_6]$ was observed to increase with the enlargement of the radius of the M component (r_M). Despite FAZT-Cs exhibiting the highest T_c, its stability was found to be poor, leading us to focus on studying FAZT-Rb in detail. Upon heating and cooling, FAZT-Rb and AZT-Rb experienced reversible phase transitions at 350 K and 218 K, respectively (Fig. 1b). The sharp peaks and large thermal hysteresis of 16 K in FAZT-Rb and 24 K in AZT-Rb suggest a distinctive feature of the first-order phase transition. Moreover, a significant enhancement of 132 K in the T_c of FAZT-Rb compared to AZT-Rb indicates that H/F substitution on AZT-Rb effectively improves T_c. Similarly, after fluorination, the T_c of FAZT-K increased from 193 K (compared to AZEFe[56]) to 295 K (Fig. S5, ESI†), the T_c of FAZT-Cs increased from 300 K to 379 K (T_{c1} of FAZT-Cs), and 394 K (T_{c2} of FAZT-Cs) (Fig. S6, ESI†), providing powerful evidence for the role played by H/F substitution. For convenience, we label the phases above 350 K for FAZT-Rb and 218 K for AZT-Rb as the high-temperature phase (HTP), and the phases below 334 and 194 K, as the low-temperature phase (LTP). The same applies to FAZT-K, AZT-K, FAZT-Cs, and AZT-Cs, but for FAZT-Cs, we introduce the intermediate-temperature phase (ITP) to describe the phase between T_{c1} and T_{c2}.

Dielectric properties

The temperature-dependent dielectric constants were measured for all compounds. As depicted in Fig. 2a, 2b, and S7 (ESI),† FAZT-K, AZT-K,[56] FAZT-Rb, AZT-Rb, and AZT-Cs all display step-like dielectric anomalies in the real part (ε') of the dielectric constant around T_c in both heating and cooling modes, indicating reversible phase transitions consistent with the DSC results. Fig. S7c (ESI)† reveals dielectric transitions around T_{c2} for FAZT-Cs, exhibiting peak-like anomaly in the heating process and damped step-like anomaly during the cooling process, suggesting its thermal instability. For instance, in LTP, the ε' of FAZT-Rb remains stable at about 6.6, while for AZT-Rb, it is approximately 5, indicating the low dielectric state. As the temperature continues to increase towards T_c, the values of ε' of FAZT-Rb and AZT-Rb dramatically increase to 33 and 20, respectively, within a narrow temperature region. In the HTP, their ε' remains almost unchanged, corresponding to the high dielectric state. Compared to AZT-Rb, which exhibits a switching ratio of 4, FAZT-Rb shows
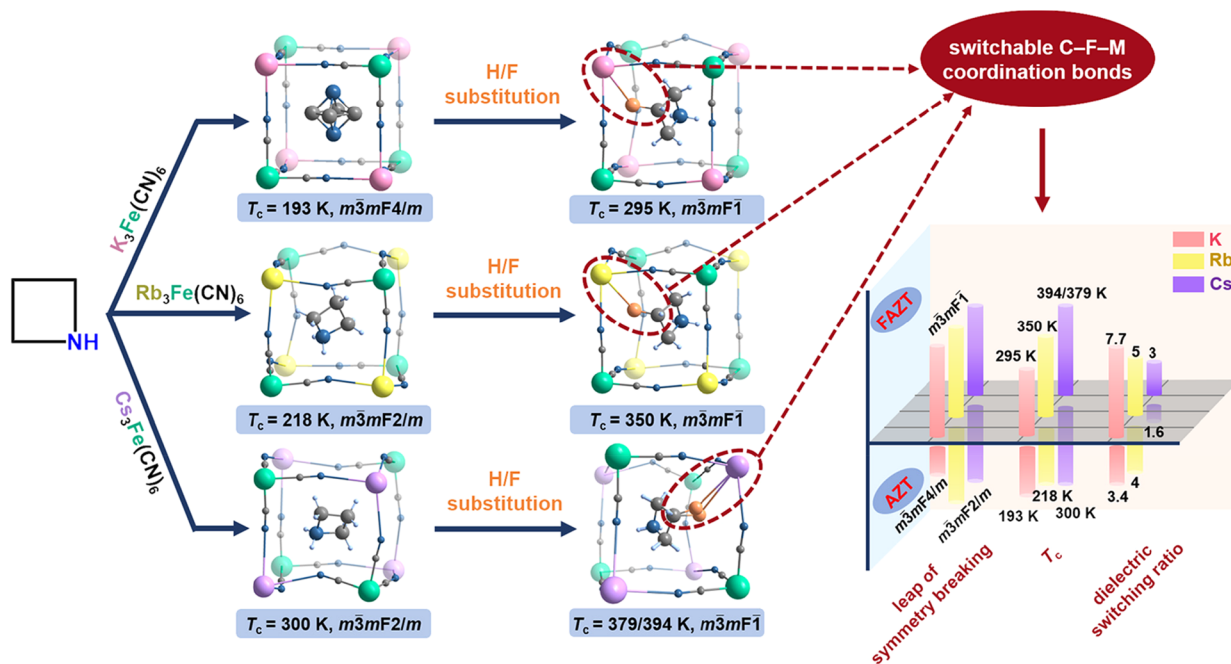
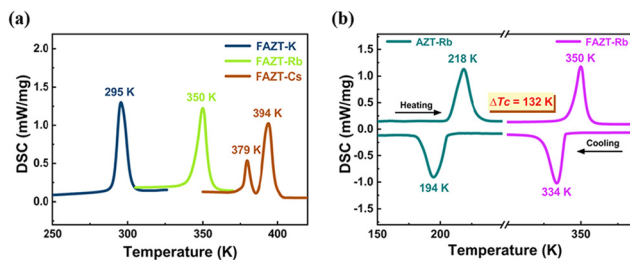**Scheme 1** Schematic strategy of H/F substitution for designing compounds FAZT-K, FAZT-Rb, and FAZT-Cs.

Fig. 1 (a) DSC curves upon heating for FAZT-K, FAZT-Rb, and FAZT-Cs and (b) DSC curves of FAZT-Rb and AZT-Rb.

Fig. 2 Temperature-dependent dielectric constants of FAZT-Rb (a) and AZT-Rb (b); reversible dielectric switching (ON and OFF) of ε' between the HTP and LTP measured for FAZT-Rb (c) and AZT-Rb (d) at 1 MHz.

an improvement after fluoridation with a ratio between high and low dielectric states of 5. As for FAZT-Cs, the ε' values are 27.5 and 9.15 at 393 and 360 K, respectively, in the heating process, and the ratio is 3 (Fig. S7c, ESI†).

As illustrated in Fig. 2c, 2d, and S8 (ESI),† for FAZT-K, AZT-K, FAZT-Rb, AZT-Rb, and AZT-Cs, ε' switching is stable and remains constant after at least five cycles. In each cycle, the low dielectric state represents "switch-off", while the high dielectric state signifies "switch-on". Their ε' undergo reciprocal and rapid changes between the low dielectric state and the high dielectric state as the temperature repeatedly crosses above or below T_c. The repetition of ON/OFF cycles suggests potential electronic applications for the compounds we studied.

Structural analyses

FAZT-K, FAZT-Rb, and FAZT-Cs were designed through H/F substitution on the azetidine cations based on AZT-K, AZT-Rb, and AZT-Cs, respectively. Their structural analysis was con-
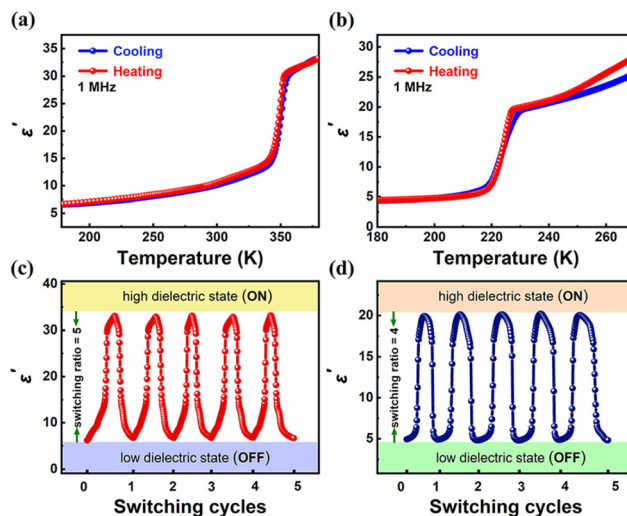
ducted using variable temperature single-crystal X-ray diffraction (XRD). Taking FAZT-Rb and AZT-Rb as examples, in the LTP, the asymmetric units of both contain two organic cations, one $[Fe(CN)_6]^{3-}$ anion, and one Rb^+ (Fig. 3a and b). Both compounds exhibit double perovskite cage structures where each Fe^{3+} ion connects six Rb^+ ions *via* CN^- linkers (Fe–C≡N–Rb), forming the 3D metal–organic framework as hosts and cations are located in the cages as guests (Fig. 3c–h). The key difference is that FAZT-Rb forms switchable C–F–Rb coordination bonds after fluorination, reducing the symmetry from the
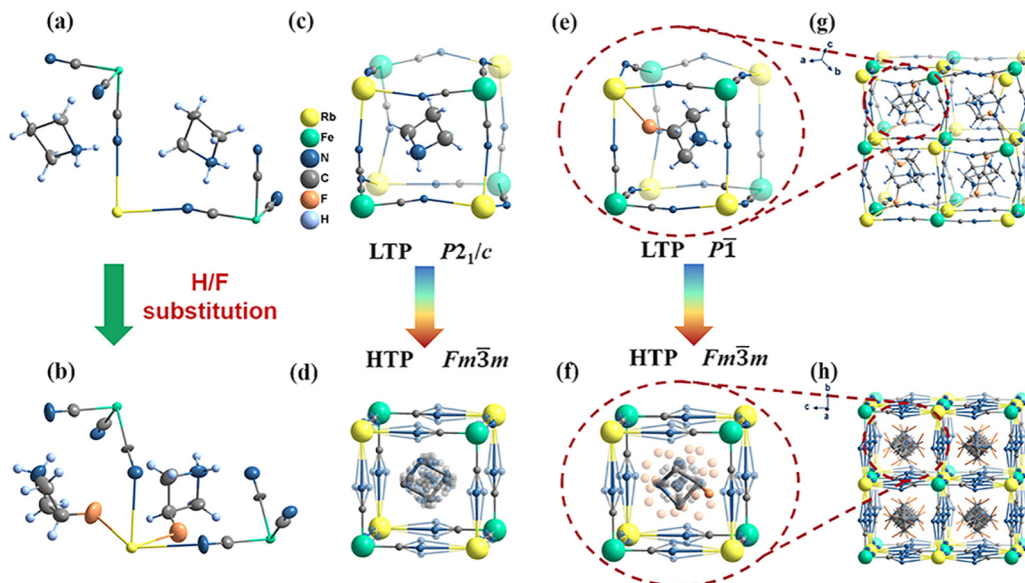
Fig. 3 Crystal structures of FAZT-Rb and AZT-Rb. The asymmetric unit in the LTP of AZT-Rb (a) and FAZT-Rb (b) is drawn as displacement ellipsoids with 50% probability. The basic unit of the framework in the LTP and HTP of AZT-Rb (c), (d) and FAZT-Rb (e), (f). Perspective view of the packing structure of FAZT-Rb in the LTP (g) and HTP (h). The hydrogen atoms in the HTP are omitted for clarity.

monoclinic $P2_1/c$ space group to the triclinic $P\bar{1}$ space group (Table S2, ESI†). In the LTP of FAZT-Rb (300 K), the perovskite cavities accommodate ordered 3-fluoroazetidine cations, which are connected to the neighboring Rb^+ ions *via* C–F–Rb coordination bonds (Fig. 3e and g). The movements of guest molecules are inhibited by the C–F–Rb coordination bonds with distances of 3.147(10) Å, accompanied by the distortion of Fe–CN–Rb bridges and slight deformation of the anionic framework (Tables S3 and S4, ESI†).

In the HTP (373 K), FAZT-Rb crystallizes in the cubic space group $Fm\bar{3}m$, with the guest molecules exhibiting a 24-fold disorder (Fig. 3f and h). The bond lengths of the metal–organic cage have identical values, resulting in an ideal octahedral geometry due to the high symmetry (Tables S3 and S4, ESI†). During the heating process, the C–F–Rb coordination bonds connecting the main framework and 3-fluoroazetidine cations are broken and the nitrogen atoms of the inorganic framework become a 4-fold disorder. Additionally, the cell volume at 300 K is smaller compared to that of the HTP. Thus, the primary structural difference between the HTP and LTP lies in the distinct motion modes of the guest molecules, as well as the slight change in the framework structure of the $[Rb_4Fe_4(CN)_{12}]$ cage. Furthermore, the order–disorder transition of 3-fluoroazetidine cations and the generation/cleavage of switchable C–F–Rb coordination bonds drive the structural phase transition at 350 K, resulting in the largest leap of symmetry breaking from a cubic paraelastic phase ($Fm\bar{3}m$) to a triclinic ferroelastic phase ($P\bar{1}$). Moreover, the cations of the AZT-Rb are highly ordered in the LTP and become dynamically disordered in the HTP (Fig. 3c and d), which is responsible for the reversible ferroelastic transition with an Aizu notation of $m\bar{3}mF2/m$. Significantly, as both FAZT-Rb and AZT-Rb under-

went order–disorder transition, the rotating motions of the organic cations generate a potential energy barrier, which may be heightened by H/F substitution, thereby enhancing T_c. As shown in Fig. S9 and S10 (ESI),† FAZT-K and FAZT-Cs exhibit a similar disordered model to FAZT-Rb in the HTP, crystallizing in the $P\bar{1}$ space group in the LTP, and experiencing the same ferroelastic phase transition as FAZT-Rb with an Aizu notation of $m\bar{3}mF\bar{1}$. Similarly, the states of AZT-K[56] and AZT-Cs resemble AZT-Rb in the HTP, but in the LTP AZT-K has a different space group from AZT-Rb, which is $P4_2/m$, while AZT-Cs shares the same space group $P2_1/c$ as AZT-Rb. Notably, the azetidine cations in the LTP of AZT-K as well as the fluorine atoms in the LTP of FAZT-Cs are disordered. In the ITP, FAZT-Cs crystallizes in the $C2/c$ space group, where partial nitrogen atoms of the host framework are disordered. The geometrical parameters of FAZT-K, AZT-K, FAZT-Cs, and AZT-Cs are summarized in Tables S5–S10 (ESI).†

Ferroelastic domains

The $m\bar{3}mF\bar{1}$ and the $m\bar{3}mF2/m$ transitions may lead to 24 and 12 possible orientation states, respectively, which exhibit characteristics of ferroelastics.[35] To validate the ferroelasticity of FAZT-K, FAZT-Rb, and AZT-Rb, polarized light microscopy was employed to observe the evolution of ferroelastic domains. Ferroelastic domains with different orientations manifest distinct patterns of light and dark under perpendicular polarized light due to their differing birefringence properties. As illustrated in Fig. 4, the crystal samples presented clearly stable interlaced stripe-like ferroelastic domains in the ferroelastic phase (FP) before reaching the T_c, including 90° ferroelastic domains. When the temperature rose above T_c at 372 K, the crystal gradually transitioned into the paraelastic phase (PP), and the ferroelastic

4650 | *Inorg. Chem. Front.*, 2024, **11**, 4647–4653

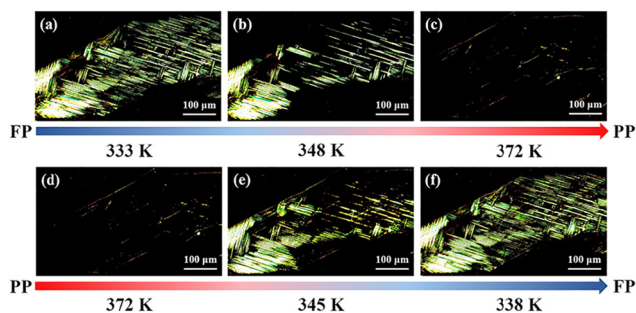This journal is © the Partner Organisations 2024

Fig. 4 Evolution of ferroelastic domains for FAZT-Rb during the heating process ((a)–(c)) and the cooling process ((d)–(f)).

domain patterns disappeared entirely, displaying uniform extinction properties owing to the high symmetry of the cubic phase. Subsequently, during the cooling process below T_c, the striped domain patterns reemerged with birefringence. The evolution of ferroelastic domains clearly demonstrates the favorable switchability of ferroelastic phase transitions. Similar ferroelastic phase transitions of AZT-Rb and FAZT-K were also observed, as shown in Fig. S11 and S12 (ESI).†

Conclusions

In conclusion, we have successfully synthesized a series of 3D cyano-bridged perovskite ferroelastics $[C_3H_5FNH_2]_2[MFe(CN)_6]$ (M = K (FAZT-K), Rb (FAZT-Rb), and Cs (FAZT-Cs)), achieving a significant enhancement of T_c. This accomplishment showcases an innovative molecular design approach utilizing a fluorine substitution strategy. FAZT-K, FAZT-Rb, and FAZT-Cs underwent structural phase transitions at around 295 K, 350 K, 379 K (T_{c1} of FAZT-Cs), and 394 K (T_{c2} of FAZT-Cs), respectively, indicating an increase in T_c with the growing radius of the M component, r_M. Among them, FAZT-Rb performs the best in T_c enhancement and dielectric switching performance, with C–F–M coordination bonds playing a pivotal role. Compared to the parent compound AZT-Rb, the introduction of C–F–Rb coordination bonds in FAZT-Rb, along with disorder–order motions of $[C_3H_5FNH_2]^+$ cations, facilitates the largest leap of symmetry breaking in 3D cyano-bridged perovskite ferroelastics, leading to the most violent structural phase transition with an Aizu notation of $m\bar{3}mF\bar{1}$. This study serves as a compelling demonstration of the effectiveness of H/F substitution as a strategy to manipulate T_c and expedite bond-switching phase transitions. It holds promise for the development of new ferroic materials with desirable switchable physical properties at the molecular level.

Data availability

The data supporting this study's findings are available from the corresponding author (Xiao-Gang Chen, e-mail: chenxg@ncu.edu.cn).

Author contributions

S.-Q. H. conceived the study and wrote the manuscript. M.-Z. L. carried out thermal and electrical experiments. J.-S. Zhou, L.-Y. Ji and Y. A. performed the general characterization studies. X.-G. Chen carried out X-ray characterization and guided this work.

Conflicts of interest

There are no conflicts to declare.

Acknowledgements

References

1 C. Wang, X. Ke, J. Wang, R. Liang, Z. Luo, Y. Tian, D. Yi, Q. Zhang, J. Wang, X.-F. Han, G. Van Tendeloo, L.-Q. Chen, C.-W. Nan, R. Ramesh and J. Zhang, Ferroelastic switching in a layered-perovskite thin film, *Nat. Commun.*, 2016, **7**, 10636.

2 Y. Hu, L. You, B. Xu, T. Li, S. A. Morris, Y. Li, Y. Zhang, X. Wang, P. S. Lee, H. J. Fan and J. Wang, Ferroelastic-switching-driven large shear strain and piezoelectricity in a hybrid ferroelectric, *Nat. Mater.*, 2021, **20**, 612–617.

3 S. H. Baek, H. W. Jang, C. M. Folkman, Y. L. Li, B. Winchester, J. X. Zhang, Q. He, Y. H. Chu, C. T. Nelson, M. S. Rzchowski, X. Q. Pan, R. Ramesh, L. Q. Chen and C. B. Eom, Ferroelastic switching for nanoscale non-volatile magnetoelectric devices, *Nat. Mater.*, 2010, **9**, 309–314.

4 X. Xiao, J. Zhou, K. Song, J. Zhao, Y. Zhou, P. N. Rudd, Y. Han, J. Li and J. Huang, Layer number dependent ferroelasticity in 2D ruddlesden–popper organic-inorganic hybrid perovskites, *Nat. Commun.*, 2021, **12**, 1332.

5 J. Li, Y. Zhu, P. Z. Huang, D. W. Fu, Q. Q. Jia and H. F. Lu, Ferroelasticity in organic–inorganic hybrid perovskites, *Chem. – Eur. J.*, 2022, **28**, e202201005.

6 H.-Y. Zhang, C.-L. Hu, Z.-B. Hu, J.-G. Mao, Y. Song and R.-G. Xiong, Narrow band gap observed in a molecular ferroelastic: Ferrocenium tetrachloroferrate, *J. Am. Chem. Soc.*, 2020, **142**, 3240–3245.

7 L.-P. Miao, L.-L. Chu, X.-B. Han, B.-D. Liang, C.-Y. Chai, C.-C. Fan, X.-X. Wang, Y.-F. Yao and W. Zhang, A ferroelastic molecular rotor crystal showing inverse temperature symmetry breaking, *Inorg. Chem. Front.*, 2021, **8**, 2809–2816.

8 Y. X. Li, Z. K. Liu, J. Cao, J. Tao and Z. S. Yao, Stress-induced inversion of linear dichroism by 4,4′–bipyridine rotation in a superelastic organic single crystal, *Angew. Chem., Int. Ed.*, 2023, **62**, e202217977.

This journal is © the Partner Organisations 2024

Inorg. Chem. Front., 2024, **11**, 4647–4653 | **4651**

9 E. J. Yoo, M. Lyu, J. H. Yun, C. J. Kang, Y. J. Choi and L. Wang, Resistive switching behavior in organic–inorganic hybrid $CH_3NH_3PbI_{3-x}Cl_x$ perovskite for resistive random access memory devices, *Adv. Mater.*, 2015, **27**, 6170–6175.

10 P.-F. Li, W.-Q. Liao, Y.-Y. Tang, H.-Y. Ye, Y. Zhang and R.-G. Xiong, Unprecedented ferroelectric–antiferroelectric–paraelectric phase transitions discovered in an organic–inorganic hybrid perovskite, *J. Am. Chem. Soc.*, 2017, **139**, 8752–8757.

11 H. Zhang, H. Wang, S. T. Williams, D. Xiong, W. Zhang, C. C. Chueh, W. Chen and A. K. Y. Jen, $SrCl_2$ derived perovskite facilitating a high efficiency of 16% in hole–conductor–free fully printable mesoscopic perovskite solar cells, *Adv. Mater.*, 2017, **29**, 1606608.

12 C.-Y. Su, Y.-F. Yao, Z.-X. Zhang, Y. Wang, M. Chen, P.-Z. Huang, Y. Zhang, W.-C. Qiao and D.-W. Fu, The construction of a two-dimensional organic–inorganic hybrid double perovskite ferroelastic with a high T_c and narrow band gap, *Chem. Sci.*, 2022, **13**, 4794–4800.

13 B. Chen, R. Yu, G. Xing, Y. Wang, W. Wang, Y. Chen, X. Xu and Q. Zhao, Dielectric engineering of 2D organic–inorganic hybrid perovskites, *ACS Energy Lett.*, 2023, **9**, 226–242.

14 B.-W. Deng, Z.-P. Rao, M.-J. Shen, K.-W. Liang, Y. Zhu, Z.-J. Wang, K. Ding, C.-Y. Su, M.-M. Lun, Z.-X. Zhang, Y. Zhang and D.-W. Fu, Homochirality to design high-T_c lead-free ferroelastic semiconductors, *J. Mater. Chem. C*, 2024, **12**, 6098–6105.

15 X.-G. Chen, Y.-Y. Tang, H.-P. Lv, X.-J. Song, H. Peng, H. Yu, W.-Q. Liao, Y.-M. You and R.-G. Xiong, Remarkable enhancement of piezoelectric performance by heavy halogen substitution in hybrid perovskite ferroelectrics, *J. Am. Chem. Soc.*, 2023, **145**, 1936–1944.

16 X.-G. Chen, X.-J. Song, Z.-X. Zhang, P.-F. Li, J.-Z. Ge, Y.-Y. Tang, J.-X. Gao, W.-Y. Zhang, D.-W. Fu, Y.-M. You and R.-G. Xiong, Two-dimensional layered perovskite ferroelectric with giant piezoelectric voltage coefficient, *J. Am. Chem. Soc.*, 2019, **142**, 1077–1082.

17 X.-G. Chen, X.-J. Song, Z.-X. Zhang, H.-Y. Zhang, Q. Pan, J. Yao, Y.-M. You and R.-G. Xiong, Confinement-driven ferroelectricity in a two-dimensional hybrid lead iodide perovskite, *J. Am. Chem. Soc.*, 2020, **142**, 10212–10218.

18 M. Takahashi, N. Hoshino, K. Sambe, T. Takeda and T. Akutagawa, Dynamics of chiral cations in two-dimensional CuX_4 and PbX_4 perovskites (X = Cl and Br), *Inorg. Chem.*, 2020, **59**, 11606–11615.

19 C. Q. Yang, R. Zhi, M. U. Rothmann, Y. Y. Xu, L. Q. Li, Z. Y. Hu, S. Pang, Y. B. Cheng, G. Van Tendeloo and W. Li, Unveiling the intrinsic structure and intragrain defects of organic–inorganic hybrid perovskites by ultralow dose transmission electron microscopy, *Adv. Mater.*, 2023, **35**, 2211207.

20 Y. Li, T. Yang, X. Liu, S. Han, J. Wang, Y. Ma, W. Guo, J. Luo and Z. Sun, A chiral lead-free photoactive hybrid material with a narrow bandgap, *Inorg. Chem. Front.*, 2020, **7**, 2770–2777.

21 M. A. Asghar, S. Zhang, T. Khan, Z. Sun, A. Zeb, C. Ji, L. Li, S. Zhao and J. Luo, Reversible phase transition driven by order–disorder transformations of metal-halide moieties in $[(C_6H_{14})NH_2]_2 \cdot CuBr_4$, *J. Mater. Chem. C*, 2016, **4**, 7537–7540.

22 S. Yan, W. Tian, H. Chen, K. Tang, T. Lin, G. Zhong, L. Qiu, X. Pan and W. Wang, Synthesis of 0D manganese–based organic–inorganic hybrid perovskite and its application in lead–free red light–emitting diode, *Adv. Funct. Mater.*, 2021, **31**, 2100855.

23 G. Y. Lee, M. Y. Yang, D. H. Kim, J. Lim, J. Byun, D. S. Choi, H. J. Lee, Y. S. Nam, I. D. Kim and S. O. Kim, Nitrogen–dopant–induced organic–inorganic hybrid perovskite crystal growth on carbon nanotubes, *Adv. Funct. Mater.*, 2019, **29**, 1902489.

24 M. Wang and S. Lin, Anisotropic and ultralow phonon thermal transport in organic–inorganic hybrid perovskites: Atomistic insights into solar cell thermal management and thermoelectric energy conversion efficiency, *Adv. Funct. Mater.*, 2016, **26**, 5297–5306.

25 T.-M. Guo, F.-F. Gao, Y.-J. Gong, Z.-G. Li, F.-X. Wei, W. Li and X.-H. Bu, Chiral two-dimensional hybrid organic-inorganic perovskites for piezoelectric ultrasound detection., *J. Am. Chem. Soc.*, 2023, **145**, 22475–22482.

26 K. Li, Z.-G. Li, J. Xu, Y. Qin, W. Li, A. Stroppa, K. T. Butler, C. J. Howard, M. T. Dove, A. K. Cheetham and X.-H. Bu, Origin of ferroelectricity in two prototypical hybrid organic-inorganic perovskites, *J. Am. Chem. Soc.*, 2022, **144**, 816–823.

27 X.-Q. Xu, H. Zhang, X.-Q. Huang and Y.-L. Liu, A high-temperature halide perovskite molecular ferroelastic with evident dielectric switching, *Inorg. Chem. Front.*, 2021, **8**, 1197–1204.

28 M. Rok, G. Bator, B. Zarychta, B. Dziuk, D. K. Skałecki, W. Medycki and M. Zamponi, Screening ferroelastic transitions in switchable cyano-bridged perovskites: $[CH_3C(NH_2)_2]_2[KM(CN)_6]$, M = Cr^{3+}, Fe^{3+}, Co^{3+}. Crystal structure characterization, dielectric properties, 1 h nmr, and quasielastic neutron scattering studies, *Cryst. Growth Des.*, 2019, **19**, 4526–4537.

29 M. Rok, B. Zarychta, M. Moskwa, B. Dziuk, W. Medycki and G. Bator, Structural phase transitions coupled with prominent dielectric anomalies and dielectric relaxation in $[(CH_3)_3NH]_2[KCo(CN)_6]$ and mixed $[(CH_3)_3NH]_2[KFe_xCo_{1-x}(CN)_6]$ double perovskite hybrids, *Dalton Trans.*, 2020, **49**, 1830–1838.

30 T. Zhang, K. Ding, J. Y. Li, G. W. Du, L. L. Chu, Y. Zhang and D. W. Fu, Hydrogen–bonded engineering enhancing phase transition temperature in molecular perovskite ferroelastic, *Chin. J. Chem.*, 2022, **40**, 1559–1565.

31 M. Wojciechowska, A. Gągor, A. Piecha-Bisiorek, R. Jakubas, A. Ciżman, J. K. Zaręba, M. Nyk, P. Zieliński, W. Medycki and A. Bil, Ferroelectricity and ferroelasticity in organic inorganic hybrid (pyrrolidinium)$_3$[Sb$_2$Cl$_9$], *Chem. Mater.*, 2018, **30**, 4597–4608.

32 M. Moskwa, P. Sobieszczyk, J. W. Mikurenda, P. Zieliński and M. Rok, Improper ferroelastic phase transition in a

4652 | *Inorg. Chem. Front.*, 2024, **11**, 4647–4653

This journal is © the Partner Organisations 2024

hydrogen-bonded metallocyanide-based (azetidinium)$_2$(H$_3$O)[Co(CN)$_6$] framework, *Chem. Commun.*, 2023, **59**, 5535–5538.

33 Z. Wu, S. Li, Y. M. Yousry, W. P. D. Wong, X. Wang, T. Ma, Z. Chen, Y. Shao, W. H. Liew, K. Yao, F. Pan and K. P. Loh, Intercalation-driven ferroelectric-to-ferroelastic conversion in a layered hybrid perovskite crystal, *Nat. Commun.*, 2022, **13**, 3104.

34 T. Y. Ju, C. C. Fan, B. D. Liang, C. D. Liu, M. L. Jin, C. Y. Chai and W. Zhang, Chirality triggered biferroicity in a 3D rubidium based perovskite, *Adv. Funct. Mater.*, 2024, 2316747, DOI: 10.1002/adfm.202316747.

35 M. Trzebiatowska, A. Gągor, L. Macalik, P. Peksa and A. Sieradzki, Phase transition in the extreme: A cubic-to-triclinic symmetry change in dielectrically switchable cyanide perovskites, *Dalton Trans.*, 2019, **48**, 15830–15840.

36 M. Trzebiatowska, M. Mączka, A. Gagor and A. Sieradzki, Pyrrolidinium-based cyanides: Unusual architecture and dielectric switchability triggered by order–disorder process, *Inorg. Chem.*, 2020, **59**, 8855–8863.

37 Z. Cai, X.-N. Hua, Y. Zhang, J. Chen, K. Sun, Z. Wang, X. Liu, X. Zhang, S. Xiao and B. Sun, Structural phase transition and dielectric responses in two novel cyano-bridged coordination polymers synthesized by sealing the incomplete cyano-bridged cage, *Inorg. Chem. Front.*, 2023, **10**, 5320–5327.

38 W.-J. Xu, K.-P. Xie, Z.-F. Xiao, W.-X. Zhang and X.-M. Chen, Controlling two-step phase transitions and dielectric responses by A-site cations in two perovskite-like coordination polymers, *Cryst. Growth Des.*, 2016, **16**, 7212–7217.

39 W. Zhang, Y. Cai, R.-G. Xiong, H. Yoshikawa and K. Awaga, Exceptional dielectric phase transitions in a perovskite-type cage compound, *Angew. Chem., Int. Ed.*, 2010, **49**, 6608–6610.

40 K. Qian, F. Shao, Z. Yan, J. Pang, X. Chen and C. Yang, A perovskite-type cage compound as a temperature-triggered dielectric switchable material, *CrystEngComm*, 2016, **18**, 7671–7674.

41 Y. Mao, X. G. Chen, Z. X. Gu, Z. X. Zhang, X. J. Song, N. Gu and R. G. Xiong, Homochiral multiferroic cyanido–bridged dimetallic complexes assembled by C−F···K interactions, *Angew. Chem., Int. Ed.*, 2022, **61**, e202204135.

42 M. Rok, J. K. Prytys, V. Kinzhybalo and G. Bator, Flexible crystals of perovskite-like coordination polymers with a tunable and switchable organic guest: (CH$_3$NH$_3$)$_2$[KFe(CN)$_6$] and (CH$_3$NH$_3$)$_2$[KCo(CN)$_6$], *Dalton Trans.*, 2017, **46**, 2322–2331.

43 W. Zhang, H.-Y. Ye, R. Graf, H. W. Spiess, Y.-F. Yao, R.-Q. Zhu and R.-G. Xiong, Tunable and switchable dielectric constant in an amphidynamic crystal, *J. Am. Chem. Soc.*, 2013, **135**, 5230–5233.

44 X. Zhang, X.-D. Shao, S.-C. Li, Y. Cai, Y.-F. Yao, R.-G. Xiong and W. Zhang, Dynamics of a caged imidazolium cation– toward understanding the order-disorder phase transition

and the switchable dielectric constant, *Chem. Commun.*, 2015, **51**, 4568–4571.

45 M.-Z. Li, Z.-H. Chen, S.-Q. Hu, J.-S. Zhou, L.-Y. Ji and X.-G. Chen, Hydrogen-bonding engineering in a 3D cyano-bridged double-perovskite ferroelastic greatly improves the phase-transition temperature, *J. Mater. Chem. C*, 2023, **11**, 15952–15958.

46 W.-J. Xu, P.-F. Li, Y.-Y. Tang, W.-X. Zhang, R.-G. Xiong and X.-M. Chen, A molecular perovskite with switchable coordination bonds for high-temperature multiaxial ferroelectrics, *J. Am. Chem. Soc.*, 2017, **139**, 6369–6375.

47 M. Rok, A. Ciżman, B. Zarychta, J. K. Zaręba, M. Trzebiatowska, M. Mączka, A. Stroppa, S. Yuan, A. E. Phillips and G. Bator, Cyano-bridged perovskite [(CH$_3$)$_3$NHO]$_2$[KM(CN)$_6$], [M: Fe(iii), and Co(iii)] for high-temperature multi-axial ferroelectric applications with enhanced thermal and nonlinear optical performance, *J. Mater. Chem. C*, 2020, **8**, 17491–17501.

48 X.-G. Chen, Z.-X. Zhang, Y.-L. Zeng, S.-Y. Tang and R.-G. Xiong, H/F substitution induced switchable coordination bonds in a cyano-bridged hybrid double perovskite ferroelastic, *Chem. Commun.*, 2022, **58**, 3059–3062.

49 Y. Ai, H.-P. Lv, Z.-X. Wang, W.-Q. Liao and R.-G. Xiong, H/F substitution for advanced molecular ferroelectrics, *Trends Chem.*, 2021, **3**, 1088–1099.

50 Y.-L. Liu, S.-Q. Lu, Y.-Y. Tang, X.-G. Chen, J.-X. Gao, H.-J. Li and R.-G. Xiong, Fluorination observedtcincrease of 110 K is challenging the hydrogen–deuterium isotope effect, *Chem. Commun.*, 2019, **55**, 10007–10010.

51 Y. Y. Tang, Y. Ai, W. Q. Liao, P. F. Li, Z. X. Wang and R. G. Xiong, H/F–substitution–induced homochirality for designing high–T_c molecular perovskite ferroelectrics, *Adv. Mater.*, 2019, **31**, 1902163.

52 J.-Q. Gan, Z.-K. Xu, T. Gan, Y. Qin and Z.-X. Wang, Large phase-transition temperature enhancement achieved in a layered lead iodide hybrid crystal by H/F substitution, *Inorg. Chem.*, 2023, **62**, 14469–14476.

53 Y. Y. Tang, Y. Xie, Y. L. Zeng, J. C. Liu, W. H. He, X. Q. Huang and R. G. Xiong, Record enhancement of phase transition temperature realized by H/F substitution, *Adv. Mater.*, 2020, **32**, 2003530.

54 Y. Ai, X.-G. Chen, P.-P. Shi, Y.-Y. Tang, P.-F. Li, W.-Q. Liao and R.-G. Xiong, Fluorine substitution induced high tc of enantiomeric perovskite ferroelectrics: (*R*)- and (*S*,)-3-(fluoropyrrolidinium)MnCl$_3$, *J. Am. Chem. Soc.*, 2019, **141**, 4474–4479.

55 Y. Ai, D.-J. Wu, M.-J. Yang, P. Wang, W.-H. He and W.-Q. Liao, Highest-T_c organic enantiomeric ferroelectrics obtained by F/H substitution, *Chem. Commun.*, 2020, **56**, 7033–7036.

56 M. Rok, M. Moskwa, J. Hetmańczyk, Ł. Hetmańczyk and G. Bator, Switchable dielectric constant, structural and vibrational studies of double perovskite organic–inorganic hybrids: (azetidinium)$_2$[KCr(Cn)$_6$] and (azetidinium)$_2$[KFe(Cn)$_6$], *CrystEngComm*, 2022, **24**, 4932–4939.

This journal is © the Partner Organisations 2024

Inorg. Chem. Front., 2024, **11**, 4647–4653 | **4653**